ELSEVIER

J. Non-Newtonian Fluid Mech. 146 (2007) 11–21

Journal of Non-Newtonian Fluid Mechanics

www.elsevier.com/locate/jnnfm

Flow of entangled wormlike micellar fluids: Mesoscopic simulations, rheology and μ-PIV experiments

E.S. Boek [a,*], J.T. Padding [a,b], V.J. Anderson [a], W.J. Briels [b], J.P. Crawshaw [a]

[a] *Schlumberger Cambridge Research, High Cross, Madingley Road, Cambridge CB3 0EL, UK*

[b] *Computational Biophysics, Department of Science and Technology, University of Twente, P.O. Box 217, 7500 AE Enschede, The Netherlands*

Received 26 June 2006; received in revised form 23 October 2006; accepted 9 November 2006

Abstract

There is a great need for understanding the relationship between the structure and chemistry of surfactants forming wormlike micelles, and their macroscopic flow properties. Available macroscopic Rheological Equations of State (REoS) are often inadequate to predict flow behaviour in complex geometries or even to describe the full set of rheological measurements. In this paper, we show how the link between surfactant structure and rheology can be explored through the use of mesoscopic particulate simulations. We describe the development of a realistic Brownian Dynamics model, where the persistence length of the micelle is the smallest length scale. Most of the parameters for the BD model are obtained from atomistic Molecular Dynamics simulations to establish the link to the chemistry of the surfactant. As a preliminary result, we calculate the shear viscosity of a solution of entangled wormlike micelles as a function of increasing shear rate. The results can be approximately mapped on an experimental flow curve for this particular system, using a mean field scaling relationship. Finally, as our motivation in this work is to understand the flow of wormlike micellar fluids in porous media, we give *preliminary* experimental results for the flow in an expansion-contraction capillary using micro Particle Image Velocimetry (μ-PIV). This demonstrates the complex response of these fluids in non-viscometric flows and the challenges they pose to any predictive simulation model.

Keywords: Wormlike micelles; Rheology; Entanglements; Constitutive equation; Molecular Dynamics; Brownian Dynamics; Complex fluids

1. Introduction

Surfactant molecules in aqueous salt solutions may self-assemble reversibly into wormlike micelles. Above the overlap concentration, the viscosity of the resulting solution increases steeply with increasing surfactant concentration [1]. This creates highly viscous, shear thinning fluids with viscoelastic behaviour [2,3]. In the presence of oil, the wormlike micelles reassemble into spherical form, resulting in a low viscosity Newtonian fluid. This responsive behaviour makes viscoelastic surfactant (VES) solutions, operating in the wormlike micellar regime, ideal for many industrial applications, such as hydraulic fracturing operations in the oilfield [4].

In several applications, the flow of wormlike micellar fluids in porous media is important. For this purpose, a reliable Rheological Equation of State (REoS) is required, providing the relation between stress and shear rate at the continuum scale. Various REoS are available in the literature [5,6], but none of them is able to predict flow behaviour in complex geometries or even to give a satisfactory explanation for the full set of rheological experiments that we have made [7]. This will be elaborated further in Section 2. Moreover, and this applies to *all* REoS, the parameters depend in an unknown fashion on the particular chemistry of the surfactants, concentration and temperature. Therefore, despite the large amount of experimental data on particular surfactant systems, there is no systematic way to design fluids with a particular desired rheology. In this paper, we will show how particulate simulation methods can be used to predict rheology from first principles.

It is impossible to reach large enough length and time scales to determine the macroscopic rheology using atomistic Molecular Dynamics (MD) simulation methods; therefore a mesoscopic approach is required. In the past, a generic simulation model for wormlike micelles [8] was used to calculate the rheology of wormlike micellar fluids [11,12]. In this so-called FENE-C model, the wormlike micelle is represented by beads connected

* Corresponding author. Tel.: +44 1223 325222; fax: +44 1223 467004.
E-mail address: boek@slb.com (E.S. Boek).

0377-0257/$ – see front matter © 2006 Elsevier B.V. All rights reserved.
doi:10.1016/j.jnnfm.2006.11.002

by springs which can reversibly break. In the later FENE-CB model [9], scission plus bending stiffness were included in order to handle semi-flexibility and to prevent ring formation for systems featuring non-unimolecular scission events. In both the FENE-C and FENE-CB models, the solvent is represented by similar, but unconnected beads. The essential physics of a wormlike micelle is therefore captured without making any reference to the actual chemistry. This can sometimes be an advantage. However, the disadvantage of any generic model is that the details of the interactions between the wormlike micelles may not be very realistic. For example, for FENE-C wormlike micellar solutions at high concentrations, it was found that the recombination kinetics are diffusion-controlled[1] and dominated by self-recombination events.[2]

In contrast, for most realistic wormlike micelles, the recombination kinetics are reaction limited [11,13]. More seriously, the shear viscosity is dominated by the contribution of the solvent beads, which have a size that is (unrealistically) similar to the micellar beads [12].[3] In real micelles, the stress is dominated by the micellar bonds and entanglements.

To overcome these difficulties, a mesoscopic Brownian Dynamics (BD) model has been developed. The input parameters for this BD model are derived from atomistic Molecular Dynamics simulations. The aim of the BD model is to realistically calculate the dynamics and rheology of an entangled solution of wormlike micelles. Such a simulation can offer new insights because the theory available for the dynamics of wormlike micelles [14] makes assumptions that cannot be directly validated by experiments. For example, the average break-up time per unit length of worm is assumed to be constant and independent of stress or shear rate. An other approximation in the theory is that no fusions occur at entanglements [16]. A mesoscopic simulation approach can check and go beyond these assumptions.

In Section 3.2, we will describe the mesoscopic simulation model and its input parameters. These are mainly the mechanical properties of a wormlike micelle, which are obtained from Molecular Dynamics simulations of a small piece of wormlike micelle. Then we will describe simulation results for a particular surfactant and concentration, for both the linear and non-linear rheology.

Finally, in Section 4, we give experimental results for the flow of wormlike micellar fluids in an expansion-contraction capillary using micro Particle Image Velocimetry (μ-PIV). We emphasize that these experimental results are preliminary and their use at this stage is mainly for a qualitative comparison.

Please note that in the three following sections, we will be using the same surfactant molecule, but at slightly different concentrations and salt types. We expect the solutions to be qualitatively similar in their rheology. For example, in Section 3.1, we use concentrations which are relatively high for the surfactant and low for the salt, for computational reasons.

2. Available continuum models are inadequate

Available continuum models have proved inadequate for modelling bulk rheological measurements of wormlike micelles [7]. For example, the shear moduli measured when oscillation is superimposed on steady shearing are not predicted well, nor is the transient stress response to steps up and down in shear rate. We will show the latter in the following.

The wormlike micellar system studied was a solution of the surfactant concentrate (a mixture of the cationic surfactant erucyl bis(hydroxyethyl)methylammonium chloride (EHAC) and 2-propanol in a 3:2 ratio (by weight)), in an aqueous solution of potassium chloride. The concentration, by mass, of the solution was 3.50% surfactant concentrate and 4.00% potassium chloride. A salt-free solution of the same surfactant concentration was also made. Bohlin Rheometers were used for all rheology measurements. A cup-and-bob was used for the majority of the measurements, a 20 mm parallel-plate was used to the measure the steady-state shear stress at high shear rates, and a double-gap system was used to measure the viscosity of the salt-free solution.

A model which has proved effective in reproducing steady shear and small amplitude oscillation data for viscoelastic surfactant solutions was proposed by Bautista et al. [6]. This model assumes that the stress τ satisfies

$$\frac{\eta}{G_0}\overset{\nabla}{\tau} + \tau = 2\eta(\mathbf{D} + \lambda_J\overset{\nabla}{\mathbf{D}}) \tag{1}$$

where η/G_0 and λ_J are relaxation times, $\overset{\nabla}{\tau}$ is the co-deformational derivative of the stress tensor, and similarly for the deformation tensor $\mathbf{D}$. The parameter η has dimensions of viscosity (but note that η only equals the shear viscosity in case of a steady shear flow). The latter is a dynamically evolving parameter, the equation of motion of which is often given in terms of the fluidity $\phi = \eta^{-1}$

$$\frac{\mathrm{d}\phi}{\mathrm{d}t} = \frac{1}{\lambda}(\phi_0 - \phi) + k(\phi_\infty - \phi)\tau : \mathbf{D}. \tag{2}$$

A fit to the experimental steady-state shear stress/shear rate curve allows ϕ_0, ϕ_∞ and the product $k\lambda$ to be determined. If the experimental shear rates are insufficiently high, it is difficult to determine ϕ_∞. The viscosity of the salt-free solution (in which the surfactant was in the spherical micellar form) was used as an approximation to $1/\phi_\infty$.

[1] This is due to the absence of an energetic barrier in the FENE-C model. Although the barrier should have little effect on static properties, we are mainly interested in dynamic properties in this paper.

[2] This is true for the original FENE-C model, which was operated at low concentrations For high concentrations, the FENE-CB model was suggested [9]. Some preliminary results of this model were made available in [10].

[3] This is due to both solvent–solvent S–S and solvent–micelle S–M interactions. However, one can still gain some insight into the micellar contribution to shear thinning using FENE-C type models. Because all contributions to the total stress tensor are available, the solvent contribution can be subtracted or analysed separately. Moreover, the flow curve for the pure Lennard-Jones (LJ) fluid is well known and shows shear thinning with a characteristic time scale below the one for a wormlike micelle. For a polymer solution, the FENE + LJ beads model is also in use and allows to test molecular theories (such as the relationship between stretch and angular momentum) very well. Certainly, it does not offer a quantitative description of the shear viscosity values, and this is the point we wish to make here.

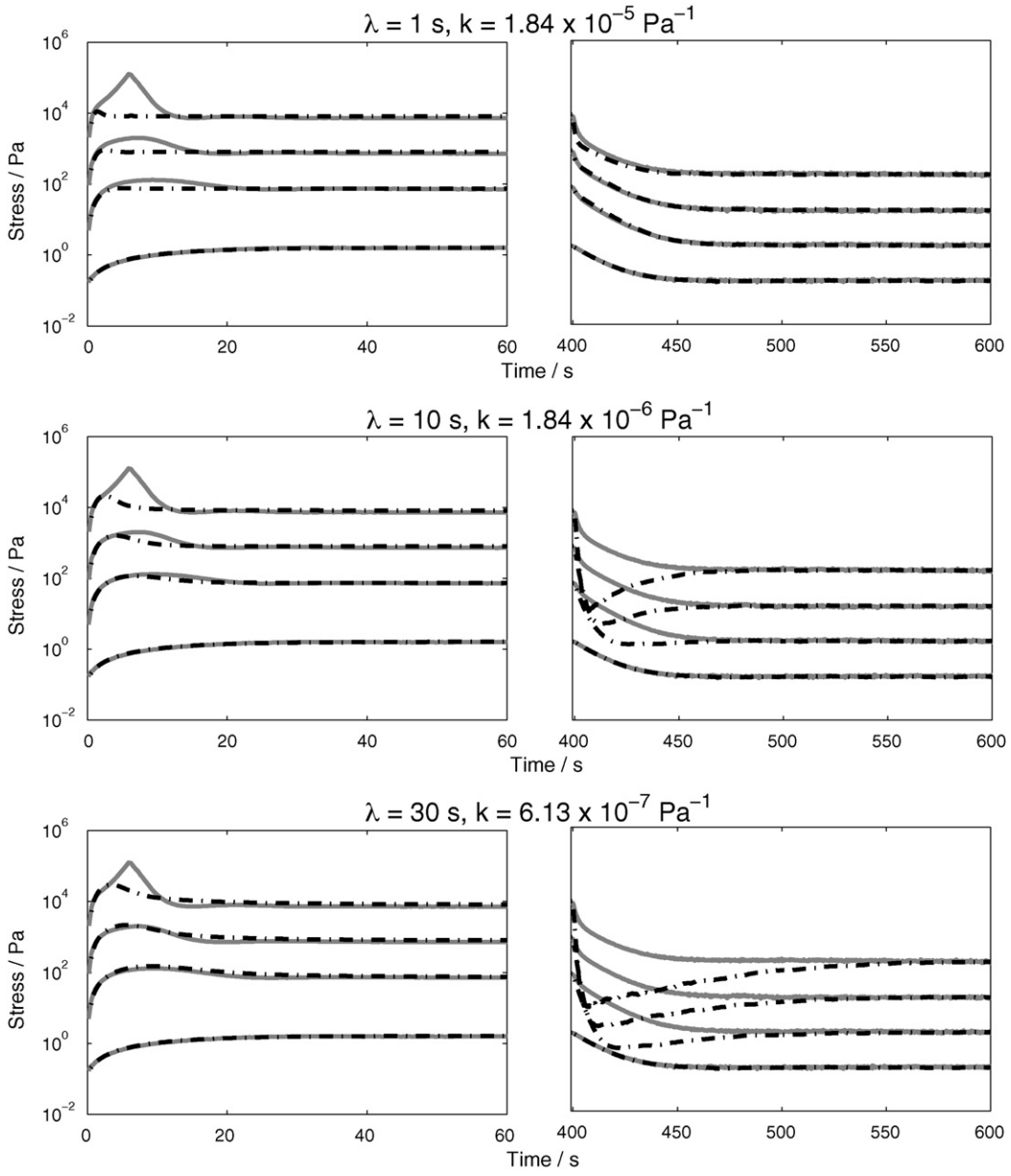

Fig. 1. Measured and predicted stress following a step increase (left) or decrease (right) in shear rate. Solid grey lines show the measured shear stress, dot-dashed lines show predictions of the BM model for $\lambda = 1$ s (top graphs), $\lambda = 10$ s (middle graphs) $\lambda = 30$ s (bottom graphs). The time origin changed such that $t = 0$ at each increase in shear rate. The curves have been shifted up the y-axis (by increasing factors of 10) for clarity. The shear rate steps are: (lowest curve) $(1.4 \times 10^{-3} \rightarrow 1.4 \times 10^{-2} \rightarrow 1.4 \times 10^{-3})$ s^{-1}, (second curve) $(1.4 \times 10^{-3} \rightarrow 3.0 \times 10^{-1} \rightarrow 1.4 \times 10^{-3})$ s^{-1}, (third curve) $(1.4 \times 10^{-3} \rightarrow 6.5 \times 10^{-1} \rightarrow 1.4 \times 10^{-3})$ s^{-1}, (top curve) $(1.4 \times 10^{-3} \rightarrow 1.4 \rightarrow 1.4 \times 10^{-3})$ s^{-1}.

Fits of the model gave

$$\eta_0 = \phi_0^{-1} = (120 \pm 7)\ \text{Pa s},$$
$$\eta_\infty = \phi_\infty^{-1} = (1.30 \pm 0.06) \times 10^{-3}\ \text{Pa s},$$
$$k\lambda = (1.84 \pm 0.184) \times 10^{-5}\ \text{Pa}^{-1}\ \text{s},$$
$$G_0 = (10.7 \pm 0.9)\ \text{Pa}$$
$$\lambda_J = (4.22 \pm 0.845)\ \text{ms}.$$

Transient measurements were made by stepping the shear rate up and down repeatedly. At each stage the shear rate was held steady until there was no significant change in the stress over a period of ≈1 min. The parameters determined above allowed predictions of transient measurements to be made for different values of λ and k (chosen such that $k\lambda$ is constant). The results are shown in Fig. 1. Predictions using a value $\lambda = \lambda_m = 1$ s fit the data obtained when the shear rate is decreased. However, a very different value $\lambda = \lambda_m = 30$ s is needed to fit those obtained when the shear rate is increased. This means that the current REoS [5,6] proves inadequate to describe the observations.

3. Multi-scale simulation model of wormlike micelles

We have developed a multi-scale particulate simulation model to calculate the rheology of wormlike micelles from

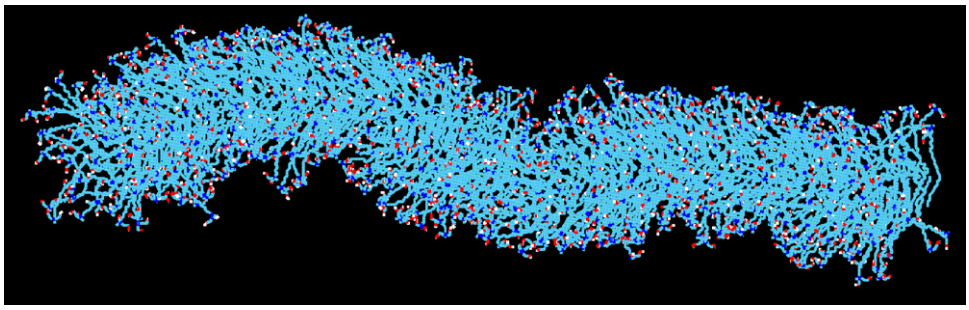

Fig. 2. Snapshot of an MD simulation of an EHAC wormlike micelle in a 3% NaCl solution. Only the surfactant molecules are shown: carbon (light blue), oxygen (red), nitrogen (dark blue) and hydrogen (white).

first principles. First, we calculate the mechanical properties of a small segment of wormlike micelles from detailed atomistic Molecular Dynamics calculations. This will be described in Section 3.1. Then we use these mechanical properties in a coarse-grained (or upscaled) mesoscopic Brownian Dynamics model of wormlike micelles, where the smallest unit is the persistence length. This will be described in Section 3.2.

3.1. Mechanical properties from Molecular Dynamics simulations

We have calculated a number of mechanical properties from detailed atomistic Molecular Dynamics simulations of a small segment of a wormlike micelle. The results of these calculations will be summarised here; for more detail, we refer to [17]. The wormlike micellar segment consists of a limited number of surfactant molecules, in this example EHAC [4]. The worm is immersed in water containing the required concentration of salt (NaCl) ions. Typically, the MD simulation box has dimensions of the order of 10 nm and contains $O(10^5)$ atoms. Periodic boundary conditions are applied in 3 dimensions so that effectively we are considering a segment of an infinite wormlike micelle. Typically, the simulations require of the order of 10 nanoseconds of simulation time to obtain statistically meaningful ensemble averages. A simulation snapshot is shown in Fig. 2. This system contains 640 surfactant and 40,000 water molecules together with Na^+ and Cl^- ions corresponding to a 3% (by weight) NaCl solution. Coulomb interactions are treated by Ewald summations.

First, we calculate radial distribution functions as ensemble averages over the particle coordinate trajectories. From these functions, we find a radius of the worm $r_w = 4.6$ nm. Second, the elastic modulus K_L is calculated from a series of simulations around the tensionless state, where we compress/stretch the worm at constant volume [18]. From the slope of the pressure difference against the worm length, we find $K_L = 1.9$ nJ/m. Third, the persistence length l_p of the worm in the tensionless state is calculated from the position fluctuation spectrum perpendicular to the worm (z-)axis. From these calculations, the persistence length is calculated to be of the order of 23 nm. This value is in agreement with experimental values for wormlike micellar persistence lengths reported in the literature [19]. In summary, the following mechanical properties will be used in the mesoscopic BD model of wormlike micelles: the radius of the worm r_w, the elastic modulus K_L and the persistence length l_p.

3.2. Mesoscopic simulation model

We have developed a Brownian Dynamics model in order to calculate the dynamics and rheology of a solution of entangled wormlike micelles. We assume that the fluid viscosity is dominated by the entanglements and therefore by the long chains. It is the strength of this mesoscopic model that we can now achieve micellar lengths comparable with the entanglement length scale. This has thus far been impossible using classic microscopic FENE models. The simulation method is based on Brownian Dynamics of coarse-grained wormlike micellar units. In our model, the entanglement and persistence lengths are two *a priori* independent quantities and we can study their relationship, e.g. as function of concentration. Each particle/unit in the simulation represents one persistence length l_p. In more detail, it represents the *midpoint* of one persistence length l_p. This is shown in Fig. 3. The endpoints of the wormlike micelles are found by extrapolating from the first and last bonds. This means that the orientation of micellar "monomers" must be traced explicitly.

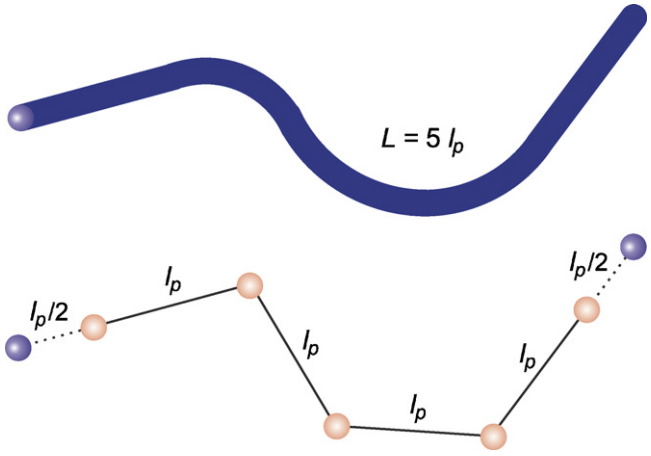

Fig. 3. Coarse-grained representation of a wormlike micelle of length $L = 5l_p$. Each unit (red sphere) represents the midpoint of one persistence length l_p. The end-points (blue spheres) of the wormlike micelles are found by extrapolating from the first and last bonds.

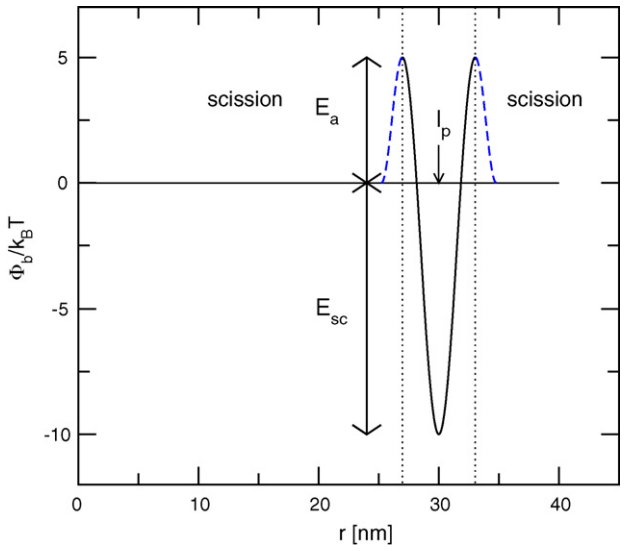

Fig. 4. Interaction energy between wormlike micellar persistence lengths l_p: there is a minimum E_{sc} (scission energy) at a distance $r = l_p$, and activation free energy barriers of height E_a.

In order to develop a realistic model of the dynamics of wormlike micelles, the following points have been taken into consideration:

(1) The ends of wormlike micelles must be able to approach each other and fuse to form elastic bonds. There is evidence that fusion in most real wormlike micelles is reaction limited [20]. Therefore, we have included a repulsive activation barrier (of tuneable height E_a), which is a function of the radial distance between two end-points. This is shown in Fig. 4.

(2) When two persistence lengths have fused, the interaction between the two midpoints is given by a potential well of tunable depth (the scission energy E_{sc}) and width (the elastic modulus K_L):

$$\Phi_b = \frac{1}{2}\frac{K_L}{l_p}(r - l_p)^2 - E_{sc} \tag{3}$$

The interaction energy landscape between two persistence lengths is given in Fig. 4.

(3) We use (overdamped) Brownian Dynamics of rigid rods of dimensions $l_p \times 2r_w$ in a solvent of viscosity η_s. The solvent friction on each particle has been made realistic by taking into account the anisotropic shape of a wormlike micelle. More precisely, the position r_i of rod i is updated according to

$$r_i(t + \Delta t) = r_i(t) + \Xi_i^{-1} \cdot F_i(t)\Delta t + v_{flow}(y)\Delta t\hat{e}_x + \Delta r_i^R, \tag{4}$$

where Δt is the integration time step, F_i the total conservative force on i, $v_{flow}(y)$ the background flow velocity (in the x direction), and Δr_i^R the random displacement, which is linked to the inverse friction (or mobility) tensor Ξ_i^{-1}, according to

$$\langle \Delta r_i \Delta r_i \rangle = 2k_B T \Xi_i^{-1} \Delta t. \tag{5}$$

Expressions for the friction tensor Ξ of a rod can be found in Ref. [21]. Here, we note that the friction perpendicular to the micelle is larger than the friction along the contour. This can be understood intuitively by realising that the friction on a rod will be smaller when the flow field is along the direction of the rod rather than perpendicular to it.

(4) In order to study shear flow, Lees-Edwards ("sliding brick") boundary conditions were implemented [24].

(5) The possibility for non-affine shear flow was included. This is not trivial for BD simulations where a friction with a static background flow $v_{flow}(y)$ is assumed. The solution was to introduce a dynamic background flow, with a velocity field coupled to the wormlike micelles through an overdamped feed back mechanism.[4]

(6) Entanglements are very important for the rheology of a concentrated solution of wormlike micelles. Entanglements emerge naturally when two wormlike micelles try to cross. In the simulation, these crossings are monitored, and entanglement points are inserted when a crossing is imminent. Essentially, the entanglement points act as sliding positions where two smooth rubber bands are in contact. This is accomplished by treating the interaction potential between two consecutive rods no longer as a function of the direct distance between the midpoints of these rods, but as a function of the *path length* between the midpoints, which may include entanglement positions. The entanglement positions are determined dynamically by enforcing a force balance on each entanglement. For more details see Refs. [22,23].

(7) Charge interactions are ignored. This means that we consider uncharged or charged systems with a small screening length as is the case for the salt concentrations used in the corresponding experiments.

(8) Excluded volume interactions are ignored. This means that we consider wormlike micelles as long thin threads. The number density of persistence length rods in the simulation is chosen equal to the number density of persistence length wormlike micelles in the experiment. In the simulation concentration comes into play only through the dynamics of entanglement formation and chain end encounters. Note that we do not consider the formation of a nematic phase.

[4] For the dynamic background flow we still assumed that the velocity field is unidirectional (in the x-direction) and homogeneous in the flow and vorticity directions. However, the dependence on the height y (the gradient direction) was determined dynamically. The feedback was accomplished by measuring, at each timestep and height y, the average "velocity" (excluding random displacements) $\langle v_{worm}(y) \rangle$ of the wormlike micellar material. The background flow velocity field $v_{flow}(y)$ reacts to this by accelerating or decelerating, depending on the difference $\langle v_{worm}(y) - v_{flow}(y) \rangle$, according to $dv_{flow}(y)/dt = 1/\tau_f(\langle v_{worm}(y) \rangle - v_{flow}(y))$ where τ_f is the flow reaction time, which was set sufficiently fast not to interfere with intrinsic timescales of the wormlike micelles. The resulting flow field is used in the following time step to determine the displacements of the wormlike micelles, etc.

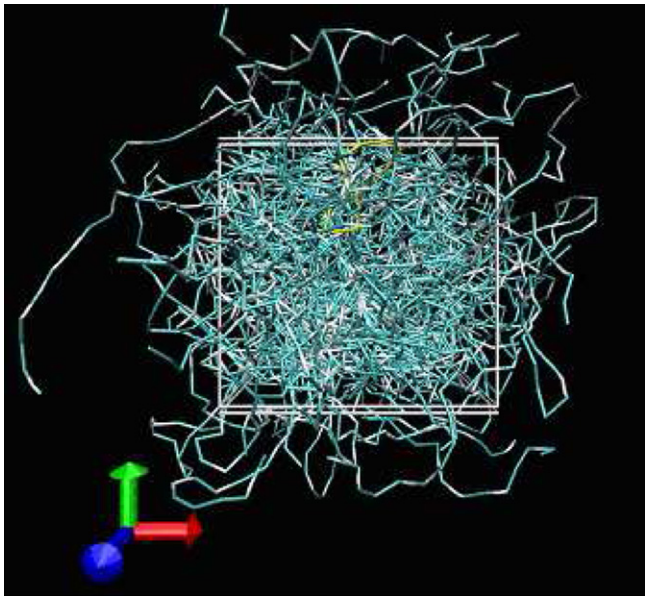

Fig. 5. Snapshot of a typical Brownian Dynamics simulation box. Wormlike micelles (blue) which penetrate the periodic planes are displayed entirely. Entanglement points are coloured white. One ring is present, which is coloured yellow.

3.3. Simulation results

A snapshot of a typical simulation box is given in Fig. 5. A typical box contains 4000–32,000 persistence length units, at a box size of 300–600 nm. This allows micellar contour lengths of O (μm). The computational speed is typically of the order of 0.1–1 ms/week on a single PC processor.

Note that we use the values of the mechanical properties given in the previous section, corresponding with a typical EHAC solution. We use water as a solvent with a viscosity $\eta_s = 10^{-3}$ Pa s. We use values of the scission and activation energies of 17 and 1.5 k_BT, respectively. These energies are the least well characterized input parameters for our system. However, rheological measurements [1] indicate a scission energy of around 25 k_BT for a similar viscoelastic surfactant fluid. High scission energies E_{sc} result in large contour lengths, associated with large simulation boxes and therefore large CPU demands. We have therefore chosen the activation energy E_a to be rather low for practicality and this will be discussed in comparison with experiment later.

First, we examine the linear (equilibrium) rheology. In the simulations, the zero-shear relaxation modulus $G(t)$ can be calculated as the ensemble average over time autocorrelations of off-diagonal elements of the stress tensor S as

$$G(t) = \frac{V}{k_BT}\langle S_{xy}(t)S_{xy}(0)\rangle \tag{6}$$

where the components of the stress tensor are defined in terms of positions r and forces F on wormlike micellar particles as

$$S_{\alpha\beta} = \frac{1}{V}\sum_{i<j}(r_{i\alpha} - r_{j\alpha})F_{i,j,\beta}. \tag{7}$$

The zero-shear viscosity then simply is the infinite time integral over the relaxation modulus [24]. A typical example of the calculation of $G(t)$ as a function of time is presented in Fig. 6.

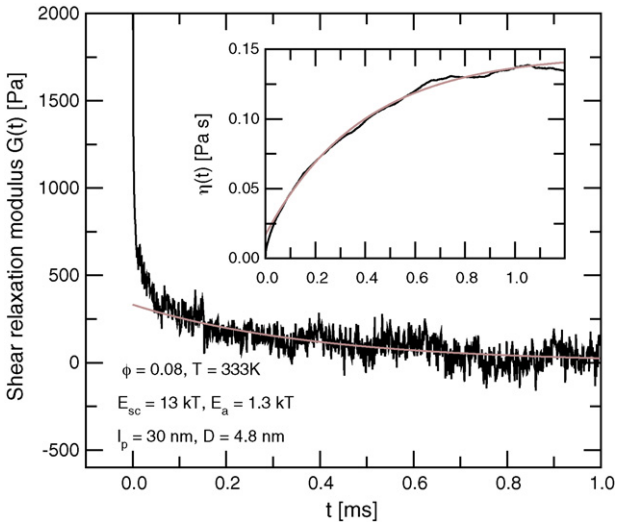

Fig. 6. Zero-shear relaxation modulus $G(t)$ as a function of time. The inset shows the time time integral of $G(t)$, which converges for infinite time.

The non-linear shear rheology, on the other hand, can be measured by applying a shear to the simulation box. When starting from an equilibrated configuration, the transient shear rheology can first be investigated. For instance, using the mesoscopic simulations, we can study the transient effect of instantaneously reducing the shear rate after initially imposing a high shear rate. A typical result is shown in Fig. 7. Initially, a shear rate of 10^6 s^{-1} is imposed, and the corresponding transient shear stress is measured. Then, the simulation is stopped and three new simulations are re-started instantaneously at shear rates lower than the original value, at 10^5, 10^4 and 10^3 s^{-1}, respectively. From Fig. 7, it can be observed that the transient time required to recover the steady shear stress at that shear rate, increases with decreasing shear rate. Also, the shear stress overshoots or undershoots depend on the secondary shear rate imposed. This

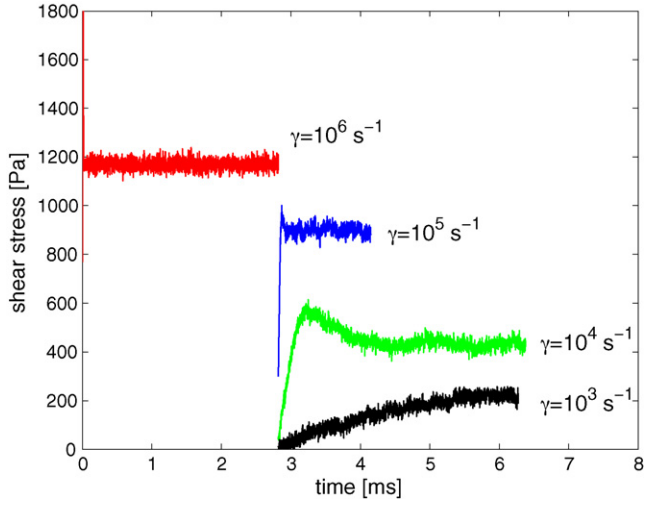

Fig. 7. Transient shear stress "recovery" as a function of time, after an initial shear rate of 10^6 s^{-1} (red), for three different values of the secondary shear rate, varying from 10^5 (blue), 10^4 (green) and 10^3 s^{-1} (black).

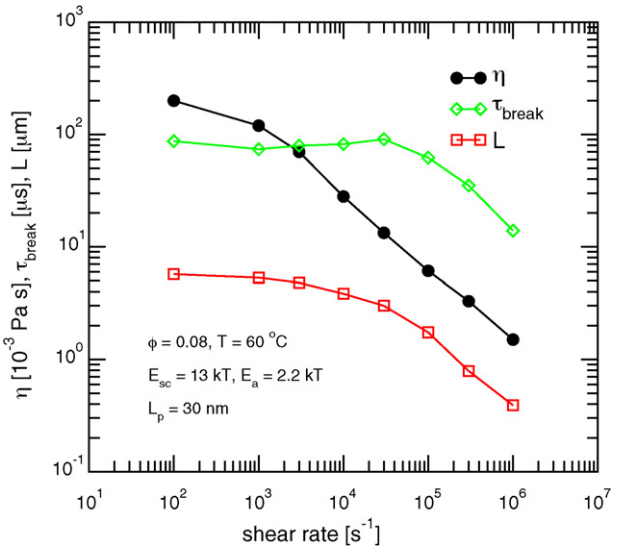

Fig. 8. Viscosity η (circles), average length L (squares) and average breaking times as a function of increasing shear rate.

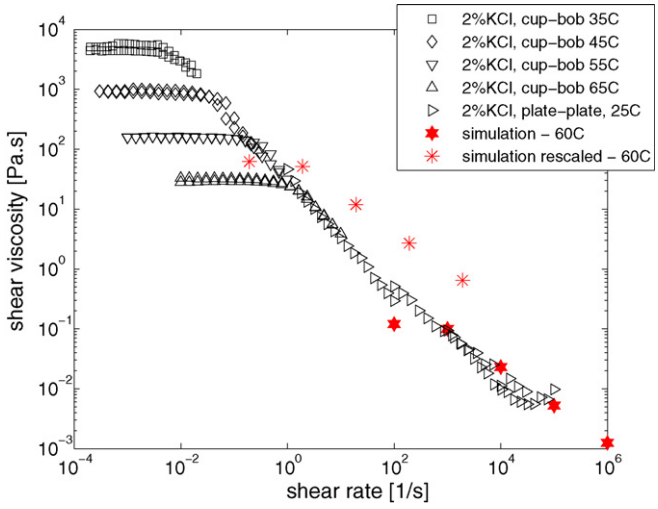

Fig. 9. Shear viscosity of 8% EHAC solutions using experiment (black symbols) and simulations (red symbols): (a) rheometer cup & bob geometry at different temperatures; (b) rheometer plate-plate geometry ($T = 25\,^{\circ}$C); (c) simulations at $T = 60\,^{\circ}$C and (d) simulation results rescaled.

is in qualitative agreement with experimental and REoS results [7]. The more rapid response in the simulation compared to the experimental data is probably a consequence of the value chosen for the activation energy which we infer to be unrealistically low.

When the simulations under shear have achieved a dynamic equilibrium, the steady-state behaviour can be studied. The steady-state shear viscosity is then given by the ratio of shear stress and shear rate:

$$\eta(\dot{\gamma}) = \lim_{t\to\infty} \frac{\langle S_{xy}(\dot{\gamma})\rangle}{\dot{\gamma}} \tag{8}$$

In Fig. 8, we show how various observables change as a function of increasing shear rate. First, we see that the viscosity decreases, as well as the average worm length. The observed shear thinning is much stronger than in the corresponding case of unbreakable polymers [25]. This is what we expect intuitively with increasing shear rate. However, we also see that the average breaking time of the worms changes with shear rate. Note that this observation is opposite to the Cates [14] mean field scaling result

$$\tau_{\text{break}}(L) = \frac{1}{c_1 L} \tag{9}$$

where c_1 is the breaking rate of one bond, which predicts an increase in the breaking time, inversely proportional to the worm length. From the simulations, we observe that under shear, the worm length L decreases as well as the breaking time.[5] We conclude that our model can go beyond the usual mean field approximation [14] which may not always be applicable. This means that one has to be very careful when deriving scission and activation energies from rheology experiments, using such mean field approximations [26].

In Fig. 9, we compare the simulation results (red symbols) with experimental measurements (black symbols) of the shear viscosity for 8% EHAC/2% KCl solutions. We show experimental data using the cup and bob geometry at relatively low shear rates, for temperatures between 35 and 65 °C. We also show experimental measurements for the same system using the plate-plate geometry, which enables us to go to significantly higher shear rates (10^4 s^{-1}). Finally, simulation results at $T = 60\,^{\circ}$C, for shear rates between 10^2 and 10^6 s^{-1} are included, shown in red symbols. It appears that the simulation shear thinning behaviour is in good agreement with experiment. Also we observe a transition to a Newtonian plateau around a shear rate of 10^3 s^{-1}.

This transition occurs at a shear rate high compared with experiment. This can be understood by realising that the scission and activation energy in the simulations are low compared with the experiment. However, the experimental results can be approximately recovered using a simple scaling argument using mean field theory, as follows:

If wormlike chains are heavily entangled, then the relaxation time τ is given by [14]

$$\tau = \sqrt{\tau_{\text{break}}(\langle L\rangle)\tau_{\text{rep}}(\langle L\rangle)}. \tag{10}$$

We know that

$$\langle L\rangle \propto \phi^{1/2}\exp\frac{E_{\text{sc}}}{2} \tag{11}$$

where $\langle L\rangle$ is the average micellar length, ϕ is now the wormlike micellar volume fraction, and E_{sc} is the scission energy in units of $k_{\text{B}}T$.[6] Assuming that the breaking rate c_1 will decrease exponentially with increasing E_{sc} and E_{a}, we find that the breaking

[5] Note that in the FENE-C model, the worm length L also decreases, but that an increasing breaking time is observed with increasing shear rate [8]. For both our model and FENE-C the product $L\tau_{\text{break}}(L)$ is decreasing with shear rate, but much more so for our model.

[6] Note that these are equilibrium results for the length of a wormlike micelle. Corrections to this equation for the FENE model, including flow-induced scission, are given in Ref. [15].

time τ_{break} in expression 9 can be rewritten as follows:

$$\tau_{break}(L) = \frac{1}{c_1\langle L\rangle} \propto \frac{1}{\langle L\rangle}\exp\left(E_{sc} + E_a\right) \propto \exp\left(\frac{E_{sc}}{2} + E_a\right). \tag{12}$$

Together with

$$\tau_{rep}(L) \propto \langle L\rangle^3 \propto \exp\left(\frac{3E_{sc}}{2}\right) \tag{13}$$

this yields

$$\tau \propto \exp\left(E_{sc} + \frac{E_a}{2}\right). \tag{14}$$

Because $\eta_0 = G_0\tau$ and G_0 does not depend on the temperature, we find

$$\eta_0 \propto \tau \propto \exp\left(E_{sc} + \frac{E_a}{2}\right). \tag{15}$$

Using this mean field scaling relation, the simulation results are mapped on the experimental results. For the scaling argument to be valid, we need

- E_{sc} to be sufficiently high to be in the entangled regime;
- E_a to be sufficiently high to ensure $\tau_e \ll \tau_{break}$ ($\langle L\rangle$), where τ_e is the entanglement time scale.

The scaling result is shown in Fig. 9, where we use experimental values of $E_a = 10\,k_BT$ and $E_{sc} = 19\,k_BT$, compared with 1.5 and 17 k_BT, respectively, in the simulations [1]. The rescaled simulation results show that the zero-shear viscosity corresponds approximately with the experimental results at 60 °C. We note that this scaling result should be used with caution in the light of our earlier observation on breaking rates. We also note that the slope of the experimental curve at high shear rates, measured using the plate-plate geometry, deviates from the typically observed −1 behaviour. Interestingly, our simulation data (before rescaling) show the same deviation at high shear rate. This behaviour seems to occur for high shear rates only, so that the rescaling may not be accurate over the whole range of shear rates.

4. Experimental measurement of flow in model porous media using micro Particle Image Velocimetry

Here, we describe preliminary results for the experimental flow of wormlike micellar fluids in a micro model, using micro Particle Image Velocimetry. The mesoscopic model described above will ultimately be developed to describe complex flow conditions, such as those encountered in flow through porous media. We therefore present the subsequent experiments as an indication of the challenges inherent in the further development of the model in this context.

A major application of the EHAC fluid under discussion is injection into the pores of rock formations in the recovery of hydrocarbon resources. This adds the problem of very complex boundary geometry to that of the complexity of the rheological response of the fluid. As one step towards this we have carried out experiments in a micro-model channel with step expansion contractions as a very simple model of a porous medium.

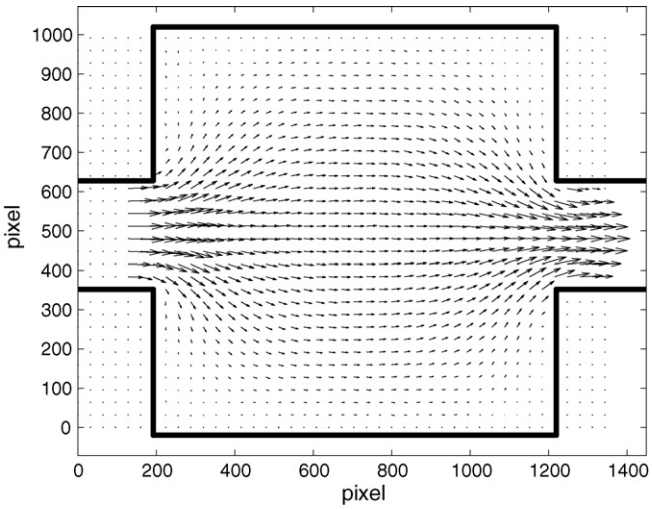

Fig. 10. Time averaged water flow field at high resolution calculated from 20 image pairs using the sum of correlation algorithm. The dark lines indicate the approximate position of the boundaries of the flow channel.

The micro-model was produced by etching a silicon wafer with the required pattern and then anodically bonding a flat glass cover to the silicon to seal the channel. Fluid connections were made by gluing a syringe needle into a slot which was ultrasonically milled into the glass cover, overlapping with the channel etched into the silicon. This process has been described in detail by Hornbrook et al. [27]. The channel was etched to a uniform depth of 40 microns and consists of a regular series of 4:1 expansion and contractions such that the narrow parts of the channel have a width of 40 microns (making the cross-section here square) and the wide parts have a width 160 microns. The length of each section is 160 microns. The duct, therefore, has dimensions comparable to the size of pores in natural rocks.

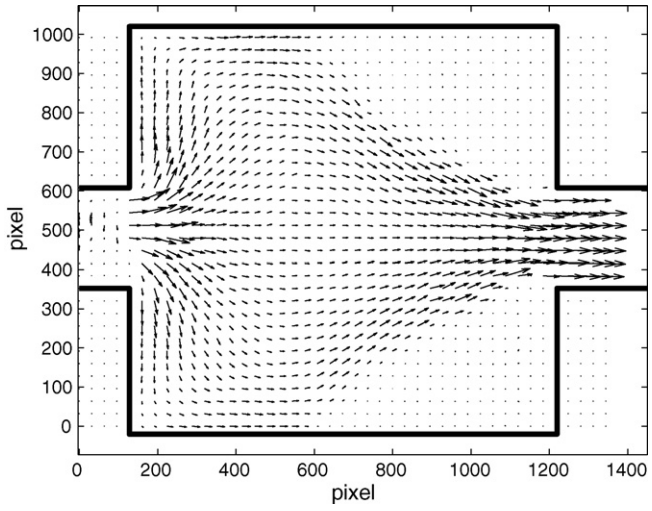

Fig. 11. Time averaged EHAC flow field at high resolution calculated from 20 image pairs using the sum of correlation algorithm.

Micro Particle Image Velocimetry was used to measure the velocity fields obtained by pumping the VES fluid through the micro channel. The μ-PIV technique is a recent adaptation [28] of particle imaging velocimetry at the macro scale. In μ-PIV, the general principle is to observe the motion of very small seeding particles by capturing image pairs with a known delay time. The velocity field is then calculated using cross-correlation algorithms. A laser is used to illuminate the entire region of interest in the micro-model through the objective lens of a microscope and excite fluorescence in the seeding particles. A plane is selected in the depth direction by moving the focal plane of the microscope objective, in our case the mid plane of the micro-channel was selected.

The μ-PIV apparatus and the image processing software were both supplied by LaVision GmbH. The seeding particles used in the study were 500 nm diameter fluorescent polymer microspheres supplied by Duke Scientific. The particles, as supplied, are charge stabilized and so tended to aggregate in the high salt concentrations used in the EHAC fluid. This is undesirable as it results in an uneven distribution of seeding and also blocking of the micro-models in extreme cases. The problem was circumvented by treating the particles with a solution of aluminium chlorohydrate, Clarient Locron P., following the method previously used by van Bruggen et al. [29] to stabilize colloidal boehmite in suspension at high salt concentrations. This process adsorbs aluminium poly-cations on the surface of the seed particles providing an additional steric stabilization. The fluid was prepared for use in the μ-PIV experiments by dispersing a concentrated suspension of the seeding particles in a EHAC solution (which was previously heated to 50 °C to reduce it's viscosity) by vigorous hand shaking. The suspension was then centrifuged at 2000 rpm for 5 min to remove the entrained air bubbles without inducing sedimentation of the seeding particles. The fluid was allowed to cool to ambient temperature before injection into the model. The concentration of the seeds was adjusted so that several in-focus particles appeared in the smallest interrogation window used in the cross-correlation processing of the images. Under the conditions of the experiment, this concentration was so low that the rheology of the fluid was unaffected. The fluid was injected into the micro-channel using as syringe pump (kd Scientific Model 789200U) to drive a 1000 μl Hamilton syringe.

Two flow experiments were carried out; a control experiment with water and the test with an EHAC fluid containing 3 wt% of

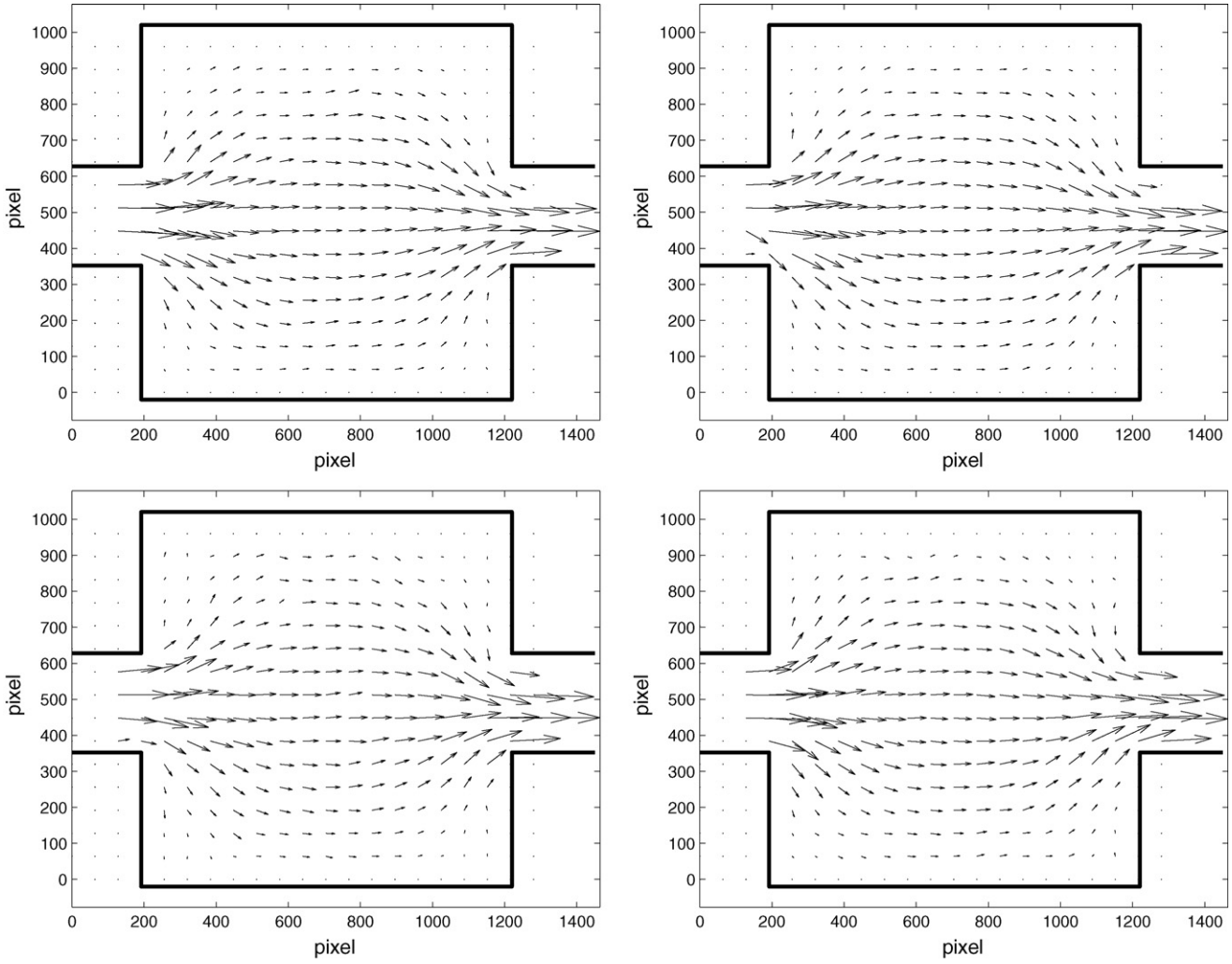

Fig. 12. Flow field of water, snapshots from single image pairs. Interval between measurements 0.2 s.

the blend of surfactant and isopropanol described in the earlier section together with 3 wt% KCl. The EHAC solution had a zero-shear viscosity of 600 Pa s at the temperature of the experiment. The flow rate in both experiments was 3 μl/min. First, we compare the flow field calculated by a "sum of correlation" algorithm using 20 image pairs. Image pairs were obtained at a frequency of 5 Hz so the vector field is averaged over around 4 s. In this technique particle image fields from each of the 20 image pairs are cross-correlated, then the ensemble average of the cross-correlation functions is calculated and finally the vector field is calculated from the averaged correlation. This gives a good signal to noise ratio at the highest resolution where there may be too few particles in some of the interrogation windows in some of the images. The result for water is shown in Fig. 10. As expected for a Newtonian fluid, the flow field is rather symmetrical and the Poiseuille profile can be seen in the narrow channel downstream. No vectors are reported in the first three interrogation windows at the end of the entry channel on the left as there was insufficient information from upstream for the vector estimation algorithm to work in this region. In the corresponding experiment with the EHAC, Fig. 11, the plug flow regime can be seen in the downstream channel and there is a large enhancement of the salient corner vortex. The velocities in the vortex are too low to be determined in this experiment which was optimized for the main flow field. A low dynamic range is an inherent feature of the PIV technique.

Time resolved vector fields can be obtained using single image pairs at the cost of increased noise and a lower resolution. In the water case the flow field is steady as shown in Fig. 12. However, in the case of the EHAC fluid, Fig. 13 shows that there were large velocity fluctuations in the region of the contraction. These velocity fluctuations are clearly not due to inertia as the relatively high viscosity of the EHAC solution ensures that the Reynolds number is much smaller than that of the corresponding experiment with water. Such instabilities are well known in the macro scale contraction flows of elastic polymer solutions [30] and the term elastic turbulence has been coined [31] for the phenomenon. The instabilities have also been observed with polymer solutions in micro fluidic devices [32]. The complexity of these flows in the pore space of natural rocks is an outstand-

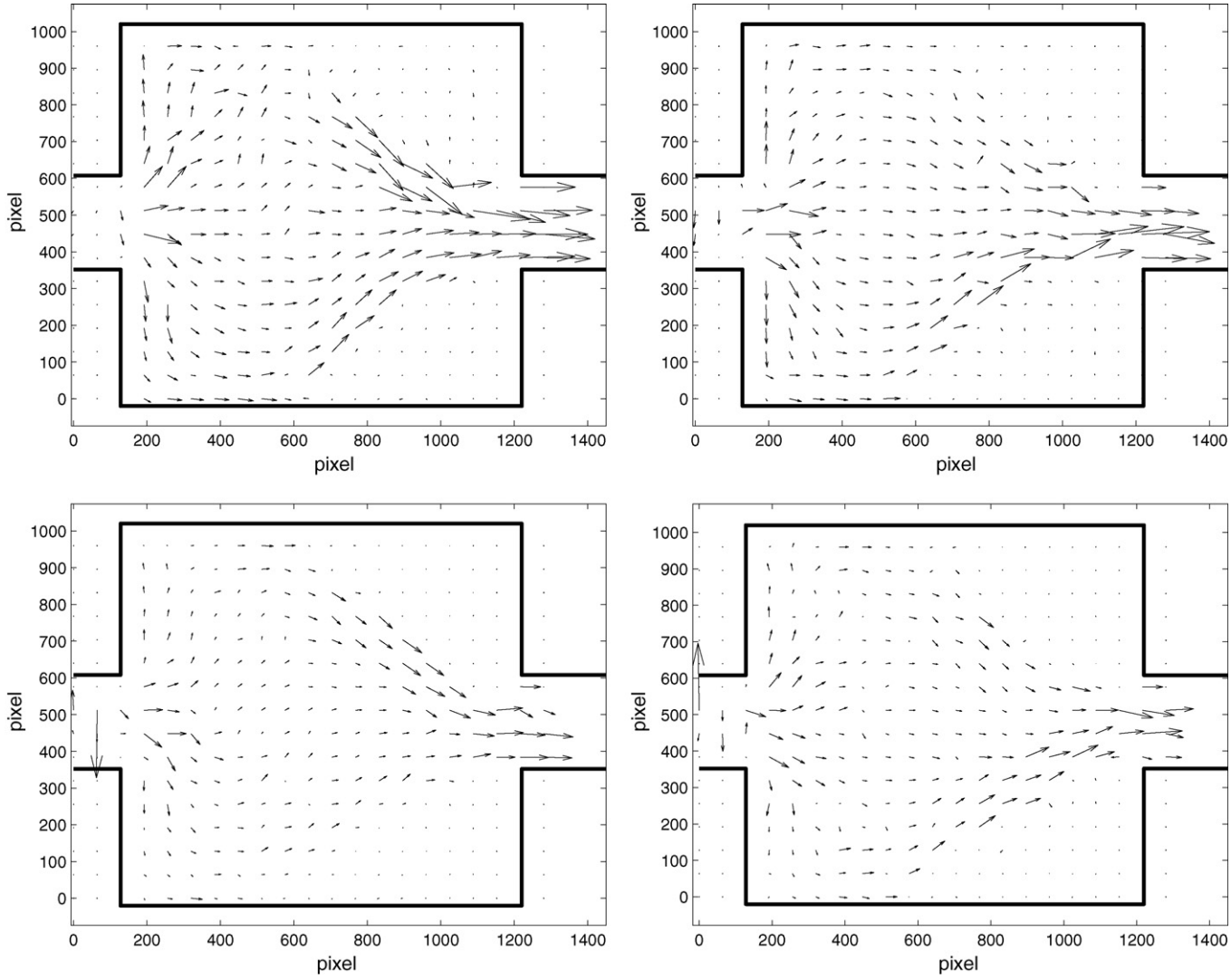

Fig. 13. Flow field of EHAC, snapshots from single image pairs. Interval between measurements 0.2 s.

ing challenge for the modelling of viscoelastic fluids, such as the EHAC solution.

5. Conclusion

In this paper, we describe experiments and numerical simulations of the flow of entangled wormlike micellar fluids. We show that the available macroscopic Rheological Equations of State, or constitutive equations, are often inadequate to describe the full set of rheological measurements. For this reason, we introduce a mesoscopic simulation model to predict the rheology of wormlike micellar fluids from first principles. The simulation model is based on the Brownian Dynamics method, using the persistence length as the smallest length scale. The parameters for the BD model, including the micellar radius, elastic modulus and persistence length are obtained from atomistic Molecular Dynamics simulations. As a preliminary result, we calculate the shear viscosity of a solution of entangled wormlike micelles as a function of increasing shear rate. The results can be approximately mapped on an experimental flow curve for this particular system, using a mean field scaling relationship. Finally, we give preliminary experimental results for the flow of wormlike micellar fluids in an expansion-contraction capillary using micro Particle Image Velocimetry. This demonstrates the complex response of these fluids in non-viscometric flows and the challenges they pose to any predictive simulation model.

Acknowledgments

We are grateful to G. Maitland and J.R.A. Pearson for helpful discussions. JTP acknowledges support from the EPSRC and IMPACT FARADAY.

References

[1] I. Couillet, T. Hughes, G. Maitland, F. Candau, S.J. Candau, Langmuir 20 (2004) 9541.
[2] M.E. Cates, S.J. Candau, J. Phys. Condens. Matter 2 (1990) 6869.
[3] S.R. Raghavan, E.W. Kaler, Langmuir 17 (2001) 300.
[4] E.S. Boek, A. Jusufi, H. Loewen, G.C. Maitland, J. Phys. Condens. Matter 14 (2002) 9413.
[5] E.S. Boek, J.T. Padding, V. Anderson, P. Tardy, J. Crawshaw, J.R.A. Pearson, J. Non-Newtonian Fluid Mech. 126 (2005) 39.
[6] F. Bautista, J.M. de Santos, J.E. Puig, O. Manero, J. Non-Newtonian Fluid Mech. 80 (1999) 93–113.
[7] V.J. Anderson, J.R.A. Pearson, J.D. Sherwood, J. Rheol. 50 (2006) 771–796.
[8] M. Kröger, R. Makhloufi, Phys. Rev. E 53 (1996) 2531.
[9] M. Kröger, Phys. Rep. 390 (2004) 453.
[10] M. Kröger, Makromol. Chetn. Macmmol. Symp. 133 (1998) 101.
[11] J.T. Padding, E.S. Boek, Europhys. Lett. 66 (2004) 756.
[12] J.T. Padding, E.S. Boek, Phys. Rev. E 70 (2004) 031502.
[13] B. O'Shaughnessy, J. Yu, Phys. Rev. Lett. 74 (1995) 4329.
[14] M.E. Cates, Macromolecules 20 (1987) 2289.
[15] W. Carl, M. Kröger, R. Makhloufi, J. Phys. France II 7 (1997) 931.
[16] W.J. Briels, P. Mulder, W.K. den Otter, J. Phys. Condens. Matter 16 (2004) S3965.
[17] J.T. Padding, E.S. Boek, W.J. Briels, J. Phys. Condens. Matter 17 (2005) S3347.
[18] E.S. Boek, W.K. den Otter, W.J. Briels, D. Iakovlev, Phil. Trans. R. Soc. Lond. A 362 (2004) 1625.
[19] L.J. Magid, J. Phys. Chem. B 102 (1998) 4064.
[20] J.T. Padding, E.S. Boek, Europhys. Lett. 66 (2004) 756.
[21] M. Doi, S.F. Edwards, The Theory of Polymer Dynamics, Clarendon, Oxford, 1986.
[22] J.T. Padding, W.J. Briels, J. Chem. Phys. 115 (2001) 2846.
[23] J.T. Padding, W.J. Briels, J. Chem. Phys. 117 (2002) 925.
[24] M.P. Allen, D.J. Tildesley, Computer Simulation of Liquids, Clarendon, Oxford, 1987.
[25] J.T. Padding, W.J. Briels, J. Chem. Phys. 118 (2003) 10276.
[26] M.E. Cates, Macromolecules 20 (1987) 2296–2300.
[27] J.W. Hornbrook, L.M. Castanier, P.A. Pettit, Observation of foam/oil interactions in a new high-resolution micromodel, in: Proc. of SPE Annual Technical Conf., 1991, SPE 22631.
[28] J.G. Santiago, S.T. Wereley, C.D. Meinhart, D.J. Beebe, R.J. Adrian, Exp. Fluids 25 (1998) 316–319.
[29] M.P.B. van Bruggen, M. Donker, H.N.W. Lekkerkerker, T.L. Hughes, Colloids Surf. A: Physicochem. Eng. Aspects 150 (1999) 115–128.
[30] R.G. Larson, Rheol. Acta 31 (1992) 213–263.
[31] A. Groisman, V. Steinberg, Nature 405 (2000) 53–55.
[32] T.M. Squires, S.R. Quake, Rev. Mod. Phys. 77 (2005) 977–1026.